Astrocyte aquaporin mediates a tonic water efflux maintaining brain homeostasis

Cuong Pham, Yuji Komaki, Anna Deàs-Just, Benjamin Le Gac, Christine Mouffle, Clara Franco, Vincent Vialou, Tomokazu Tsurugizawa, Bruno Cauli, Dongdong Li

Astrocyte aquaporin mediates a tonic water efflux maintaining brain homeostasis

Cuong Pham[1], Yuji Komaki[2], Anna Deàs-Just[1], Benjamin Le Gac[1], Christine Mouffle[1], Clara Franco[1], Vincent Vialou[1], Tomokazu Tsurugizawa[3,4,#], Bruno Cauli[1,#], Dongdong Li[1,#]

[1]Sorbonne Université, Institute of Biology Paris Seine, Neuroscience Paris Seine, CNRS UMR8246, INSERM U1130, Paris 75005, France

[2]Central Institute for Experimental Animals, Kawasaki, Japan

[3]Human Informatics and Interaction Research Institute, National Institute of Advanced Industrial Science and Technology (AIST), Tsukuba, Japan

[4]Faculty of Engineering, University of Tsukuba, Tsukuba, Japan

[#]Correspondence: tsurugizawa@hotmail.com, bruno.cauli@upmc.fr, dongdong.li@inserm.fr

Keywords: imaging, swelling, diffusion

ABSTRACT

Brain water homeostasis provides not only physical protection, but also determines the diffusion of chemical molecules key for information processing and metabolic stability. As a major type of glial cell in the brain parenchyma, astrocytes are the dominant cell type expressing aquaporin water channels. However, how astrocyte aquaporin contributes to brain water homeostasis remains to be understood. We report here that astrocyte aquaporin 4 (AQP4) mediates a tonic water efflux in basal conditions. Acute inhibition of astrocyte AQP4 leads to intracellular water accumulation as optically resolved by fluorescence-translated imaging in acute brain slices, and *in vivo* by fiber photometry in moving mice. We then show that the tonic aquaporin water efflux maintains astrocyte volume equilibrium, astrocyte and neuron Ca^{2+} signaling, and extracellular space remodeling during optogenetically induced cortical spreading depression. Using diffusion-weighted magnetic resonance imaging (DW-MRI), we observed that *in vivo* inhibition of AQP4 water efflux heterogeneously disturbs brain water homeostasis in a region-dependent manner. Our data suggest that astrocyte aquaporin, though bidirectional in nature, mediates a tonic water outflow to sustain cellular and environmental equilibrium in brain parenchyma.

Significance statement

Our brain is immersed, thus protected, in a water environment. It ensures intra- and extracellular molecular diffusion, which is vital for brain function and health. Brain water homeostasis is maintained by dynamic water transport between different cell types. Astrocytes are a main type of glial cell widely distributed in brain parenchyma, and are also the primary cell type expressing the bidirectional aquaporin water channel. Here we show that in basal conditions, aquaporin channel mediates a tonic water efflux from astrocytes. This mechanism maintains astrocyte volume stability, activity-gated brain parenchyma remodeling and brain water homeostasis. Our finding sheds light on how astrocytes regulate water states in the brain, and will help to understand brain homeostasis in specific life context.

\body

Introduction

Every aspect of brain function relies on the delicately maintained water environment. It supports brain structural stability and molecular diffusion, laying the ground for information processing, metabolite shuttling and adaptation to living environments (1). Water is the fundamental constituent of the cerebrospinal fluid infiltrating into the central nervous system and the interstitial fluid distributed in brain parenchyma (2, 3). Brain fluid transport is suggested to support the diffusion of energetic fuels like glucose and lactate to warrant the metabolic circumstances in the parenchyma, and is also implicated in the clearance of waste molecules from the brain as described in the glymphatic system (4, 5). In addition, brain water diffusion is the basis for diffusion-weighted magnetic resonance imaging (DW-MRI) for structural and functional neuroimaging (6), and for clinical diagnostics widely applied for neurological diseases such as ischemia, brain tumor and edema (7, 8).

Water equilibrium in the brain is maintained by dynamic transport between different cell entities. Aquaporin is a family of transmembrane channels facilitating bidirectional water flow, with aquaporin 4 (AQP4) being the main subtype expressed in the central nervous system. In the brain, AQP4 is predominantly expressed in astrocytes (9, 10) that are a major type of glial cells distributed throughout the parenchyma (11). This feature renders astrocytes well equipped to balance osmotic oscillations imposed by the transmembrane transport of ions, metabolites, and signaling molecules, all mediated by water. However, thus far, how astrocyte aquaporin contributes to brain water homeostasis remains elusive.

Here, combining *in vivo* chemical targeting and optical water transport imaging, we report that AQP4 sustains a tonic water efflux from astrocytes. This mechanism was found to be

critical in maintaining astrocyte volume and signaling stability, as well as the extracellular space remodeling in mouse cortex. Using DW-MRI, we observed that acute inhibition of astrocyte water efflux *in vivo* causes heterogeneous alterations in brain water diffusion. Our finding suggests that aquaporin acts as an important water export route in astrocytes, to counterbalance excessive water accumulation in the cytoplasm. This mechanism plays a necessary role in maintaining water equilibrium in astrocytes, thereby the water homeostasis in the brain.

Results

Astrocyte aquaporin mediates a tonic water efflux

To follow *in situ* astrocyte water transport, we performed fluorescence intensity-translated (FIT) imaging. To this end, mouse brain astrocytes were chemically labeled *in vivo* with a highly water-diffusible and astrocyte-specific red fluorescent dye, sulforhodamine B (SRB) (Fig. 1*A*) (12, 13). About one hour after its intraperitoneal injection, astrocytic SRB labeling was widely distributed in the mouse cortex, as seen in living acute brain slices (Fig. 1*A*) and validated by colocalization with EGFP-identified astrocytes in slices taken from GFAP-EGFP transgenic mice (Fig. 1*A*). Net water transport across the astrocyte membrane alters cytoplasmic SRB concentration and cellular volume, which can thus be followed by changes in fluorescence intensity when imaged in a fixed field of view. To validate the FIT imaging of astrocyte water transport, we employed wide-field fluorescence microscopy for single-plane time-lapse imaging in acute brain slices in the primary somatosensory (S1) cortex. This approach allowed us to collect fluorescence from both the focal plane and along the axial extensions, thereby imprinting volumetric fluorescence into the single image plane. Indeed, water influx induced by the

hypoosmotic solution caused decreases in astrocyte SRB fluorescence in a time-dependent manner which also reflected cell swelling (Fig. 1*B*); whereas water export and astrocyte shrinking upon hyperosmotic manipulation increased astrocyte fluorescence (Fig. 1*B*). Hence, FIT imaging enables real-time recording of astrocyte transmembrane water transport and volume dynamics.

In basal conditions, flat fluorescence time course was recorded suggesting equilibrated water transport across the astrocyte membrane (Fig. 1*B*) and volume homeostasis in the brain parenchyma. To inspect a tonic role of aquaporin in astrocyte water transport, we sought to acutely block the astrocyte aquaporin channel, aquaporin 4 (AQP4). We used the synthetic compound 2-(nicotinamido)-1,3,4-thiadiazole (TGN-020) that is derived from the condensation of nicotinamide and thiadiazole derivatives (14, 15), whose specificity for AQP4 has been validated *in vitro* by ion channel heterologous expression system (16) and *in vivo* using the knockout mouse model (17, 18). This approach guaranteed the functional pinpointing of astrocyte aquaporin under physiological conditions, while avoiding the chronic compensations caused by genetic tools and mouse models that have been reported to alter brain water content, volume and extracellular space potentially confounding the functional readouts (19-23).

AQP4 is a bidirectional channel facilitating passive water transport along the osmotic gradient (9). As an osmotic equilibrium is maintained in the brain parenchyma in basal state, there might not be net water transport across AQP4. However, we observed in cortical slices that acute inhibition of astrocyte AQP4 by TGN-020 gradually induced intracellular water accumulation, evidenced by a decrease in SRB fluorescence intensity as a result of cytosolic dilution (Fig. 1*C*). This observation suggests that astrocyte aquaporin mediates a tonic water efflux; its blocking causes intracellular water accumulation and swelling (Fig. 1*C, right*). To

corroborate this observation *in vivo*, we performed fiber photometry recording in moving mice (Fig. 1*D*). An optical fiber was implanted into the mouse S1 cortex to follow fluorescence signals of local astrocyte population post the intraperitoneal injection of SRB (Fig .1*D, left*). After about one hour, when astrocytes were well labeled, either saline or TGN-020 was injected intraperitoneally. While no significant effect was observed with the saline control, TGN-020 induced a decrease in astrocyte SRB fluorescence and a reduction in its oscillation range (Fig. 1*D, right*), mirroring an intracellular dilution of fluorescent molecules. This observation confirms that acute inhibition of astrocyte aquaporin leads to intracellular water accumulation thereby cell swelling.

Aquaporin inhibition perturbs astrocyte and neuron signaling

Astrocyte volume equilibrium not only determines brain architectural stability, but also associates with dynamic cellular signals. Indeed, astrocyte swelling has been shown to alter intracellular Ca^{2+} signaling (24, 25). We then performed Ca^{2+} imaging to confirm that acute aquaporin inhibition induces astrocyte swelling and thus Ca^{2+} oscillation. The genetically encoded Ca^{2+} sensor GCaMP6 was selectively expressed in astrocytes by crossing the Glast-Cre^{ERT2} and $GCaMP6^{floxP}$ mouse line (13, 26). Because astrocyte Ca^{2+} signals often occur in local domains, we adapted a light sheet microscope (13) for wide-field optical sectioning so as to image them with high signal-to-noise ratio (*SI Appendix*, Fig. S1). We first confirmed that water accumulation induced by hypotonic solution, therefore swelling, in astrocytes alters the intracellular Ca^{2+} signal (Fig. 2*A*). Then we followed astrocyte Ca^{2+} in isotonic control condition while only blocking astrocyte AQP4 with TGN-020. Ca^{2+} signaling was indeed altered upon acute inhibition of aquaporin (Fig. 2*B*), reflecting that restriction of tonic water efflux from

aquaporin leads to intracellular water accumulation, astrocyte swelling and modification of Ca^{2+} oscillation. In addition, astrocyte swelling has been reported to induce the release of neuroactive molecules such as glutamate thereby influencing nearby neuron activity (27, 28). Hence, disrupting AQP4 tonic water outflow would not only cause astrocyte swelling but also influence the activity of neighboring neurons. To validate it, we imaged Ca^{2+} signals as a surrogate for neuronal activity in cortical somatostatin (SST) interneurons which exhibit the highest excitability (29) and express both ionotropic and metabotropic glutamate receptors (30), making them ideal to sense astrocyte-released signaling molecules. We expressed GCaMP6 in SST interneurons by crossing homozygous SST-Cre (31) and homozygous $GCaMP6^{floxP}$ mice. As expected, TGN-020 inhibition of astrocyte AQP4 led to a global Ca^{2+} elevation in SST interneuron populations (Fig. 2*C*). These observations support that astrocyte aquaporin mediates a tonic water efflux, contributing to maintain both the volume and signaling homeostasis.

Aquaporin water efflux regulates astrocyte volume response

We then examined the role of aquaporin water efflux in astrocyte volume response to osmotic environments. We followed the evoked water efflux and shrinking induced by hypertonic solution. As astrocyte AQP4 supports preferentially water efflux, its inhibition would attenuate hypertonicity-imposed water extrusion (Fig. 3*A*). Supporting this, application of TGN-020 slowed down the hypertonicity-induced water efflux and shrinking, reflected by the longer time to peak in the SRB fluorescence time course as compared to control (Fig. 3*B*), though the delay in the initial onset was not significantly prolonged. The maximal increase in astrocyte SRB fluorescence was lower in the presence of TGN-020, suggesting that AQP4 blocking reduced the overall amount of water efflux (Fig. 3*B*).

We next evoked water influx, thereby astrocyte swelling, by hypotonic solution in the presence or absence of TGN-020 (Fig. 3*C*). In contrast to the effects on hypertonicity-evoked water efflux, AQP4 acute inhibition was observed to accelerate both the initial water accumulation and the swelling rate in astrocytes, reflected by their earlier onset in decrease of SRB fluorescence and the faster reaching to the plateau value relative to the control condition (Fig. 3*D*). This observation cross-validates the role of astrocyte aquaporin in supporting water efflux, whereby its blockade facilitates the evoked water accumulation (Fig. 3*C*). The maximum decrease in astrocyte SRB fluorescence was observed to be reduced with aquaporin inhibition (Fig. 3*D*). TGN-020 was present prior to hypotonic challenge, which would have slightly swelled astrocytes due to the blockade of tonic water efflux, thereby constraining the range of subsequent swelling.

Astrocytes are widely distributed throughout the brain parenchyma, orchestrating water transport and volume homeostasis (32). Water outflow via astrocyte AQP4 may play a role in the structural remodeling of parenchyma at the global level. We then induced general cell swelling by triggering cortical spreading depression (CSD) (33, 34). To be orthogonal to the pharmacological control of astrocyte aquaporin, the CSD depolarization wave was initiated by optogenetically stimulating ChR2-expressing glutamatergic cells in the cortical slices of Emx1-Cre/Ai32ChR2 mice (35, 36), termed Opto-CSD (37). As cell swelling increases the transmittance of infrared light, we imaged Opto-CSD by the intrinsic optical signal (IOS) derived from infrared illumination (34, 38). The IOS displayed transient increase across cortical layers during the Opto-CSD (Fig. 4*A*-*C*). The biphasic starting of IOS coincided with a sharp response in the extracellular potential indicating the CSD initiation (*SI Appendix*, Fig. S2*A*). IOS signal contains a first peak reflecting the rapid CSD response (Fig. 4*C*, *b*) followed by a prolonged

phase of general cellular swelling (Fig. 4*C*, *c*). By combining fluorescence imaging of SRB-labelled astrocytes, whose spectrum is separated from the IOS infrared signal, we observed that astrocytes swelling (i.e., decrease in SRB fluorescence) paralleled CSD swelling (*SI Appendix,* Fig. S3). Consistent with our observation on astrocyte volume response (Fig. 3*D*), when pre-incubating slices with TGN-020 to AQP4 tonic water outflow, the initiation of both the CSD and general swelling was accelerated while their maximum amplitude reduced (Fig. 4*D-E; SI Appendix,* Fig. S2B). Blocking action potentials with tetrodotoxin (TTX) only reduced the amplitude of the initial CSD response while the effect on general swelling is insignificant (Fig. 4*D-E*). We further followed the swelling (i.e., water influx) of SRB-labeled astrocytes during Opto-CSD. In consistence with the result obtained from hypotonic challenge (Fig. 3*D*), the pre-presence of TGN-020 reduced the peak amplitude of astrocyte swelling (Fig. 4*F*). Notably, TGN-020 significantly inhibited astrocyte recovery from the swelling state (Fig. 4*F*), indicating that blocking AQP4 hinders the water efflux required for astrocyte volume maintenance.

Collectively, our data show that astrocyte AQP4 sustains a tonic water outflow regulating the cellular volume response and the general cell swelling of parenchyma.

Tonic astrocyte water transport underlies brain homeostasis

Water homeostasis sets the basis for molecular diffusion in the brain, which instructs neurotransmitter availability, ion recycling and metabolite trafficking. We then examined *in vivo* the role of astrocyte aquaporin outflow in brain water diffusion using DW-MRI (8). It uses the diffusion of water molecules to generate contrast that can be quantified by the apparent diffusion coefficient (ADC) in the nerve tissue (39, 40). We used a 7T MRI to image global brain water diffusion in lightly anesthetized mice with medetomidine, while acutely perturbing astrocyte

AQP4 outflow by TGN-020 via intraperitoneal injection. Brain water diffusion was mapped every 5 min before and after TGN or saline (as control) administration (Fig. 5*A*). Each acquisition sweep was performed with three b values (0, 250, 1800) that accounted for ADC, so to fit the exponential curve (Fig. 5*B*). Compared to the control saline, TGN-020 significantly increased basal water diffusion within multiple regions including the cortex, hippocampus and the striatum in a heterogeneous manner (Fig. 5*C*). The temporal features in water diffusion change appeared to be also different: an early elevation followed by a reversible tendency was observed for cortical areas, a rapid and long-lasting elevation for the striatum while a delayed and transient increase for the hippocampus (Fig. 5*D*). The *in vivo* neuroimaging results confirm that the tonic water efflux from astrocyte aquaporin contributes to maintain the homeostasis of brain water diffusion, and also suggest regional and temporal heterogeneities in brain water handling.

Discussion

Water equilibrium sets the basis for brain function, plasticity and dynamics. Astrocytes are the principal brain cell type expressing aquaporin water channels that are highly implicated in maintaining local environments (10). We show that albeit being a bidirectional channel, astrocyte aquaporin sustains a tonic water outflow in basal states to ensure the structural and functional stability, as well as brain water homeostasis.

The observation of a basal aquaporin water efflux implies there is constitutive water accumulation in brain astrocytes. As a ubiquitous vehicle for transporting ions, transmitters and metabolites, water enters astrocytes via a wide range of ion channels, transporters and

exchangers. For instance, they express Na^+/K^+ and Na^+/HCO_3^- cotransporters to dynamically regulate intra- and extracellular ion homeostasis (21). Standing as a major glial cell type controlling the neuropil environment, astrocytes take up synaptically released K^+ through inwardly rectified K^+ channels and neurotransmitters (e.g., glutamate, GABA) via high-affinity transporters to safeguard synaptic transmission (41). The transmembrane molecular exchange may lead to continual water entry into astrocytes. Moreover, astrocytes juxtapose the cerebral vasculature, being a front relay station for brain metabolism. They express glucose transporter and lactate-permeable monocarboxylate transporters facilitating energy substrate uptake and transfer between blood vessels and neuron-glia networks (42). As water is produced during metabolic processes (43), astrocyte metabolism would also contribute to the constitutive water accumulation in the cytoplasm. An efficient efflux pathway appears necessary to counterbalance the excessive water buildup, thereby maintaining astrocyte and brain homeostasis. Our data suggest that astrocyte AQP4 fulfills such a role by supporting tonic water outflow (*SI Appendix*, Fig. S4). Our result echoes that in the principal cells of the kidney collecting duct, AQP4 is suggested to mainly mediate water exit to balance the AQP2-sustained water entry (44).

This study also provides mechanistic clues to understand AQP4-relevant pathologies in specific contexts. For instance, astrocyte water accumulation and swelling is a prominent cause of brain edema. The presence of AQP4 has been found to ameliorate perihematomal edema in intracerebral hemorrhage (45), which could be attributed to the contribution of AQP4 to astrocyte basal water extrusion. In neuromyelitis optica spectrum disorders, featured by circulating IgG autoantibody against AQP4, water transport ability is downregulated in astrocytes associated with swelling (46, 47). The inhibition of astrocyte AQP4 by autoantibody would reduce the tonic water efflux thereby causing progressive pathological swelling.

We observed that acutely blocking aquaporin caused basal water accumulation leading to swelling in astrocytes, and facilitated the evoked astrocyte swelling by hypoosmoticity and during cortical spreading depression. This recalls early observation by electron microscopy that knocking out the anchoring protein alpha-syntrophin to disperse AQP4 clustering induces an enlargement of astrocyte endfeet (48). It likely reflects astrocyte local swelling caused by the disruption of AQP4-mediated water efflux. Our observation also parallels the report that AQP4 knock out facilitates astrocytes swelling induced by hypoosmotic solution (49). Nevertheless, genetic inactivation of AQP4 also reveals inhibitory effects on astrocyte swelling (24, 50, 51). Such discrepancy might be due to the variable compensations in brain water content and structure integrity during chronic genetic manipulations (19-22). Astrocyte aquaporin modulates brain water transport (21), though its role in the glymphatic system is under deliberation (52-55). Our data suggest that astrocyte aquaporin-mediated outflow helps to maintain local water environment in the brain parenchyma. Moreover, besides affecting water transport, targeting AQP4 also impacts astrocyte volume therefore the size of extracellular space. These two factors would need be considered when evaluating AQP4 involvement in brain fluid transport.

We show by DW-MRI that water transport by astrocyte aquaporin is critical for brain water homeostasis. When blocking AQP4 with TGN-020, therefore its basal water outflow, we observed spatially heterogeneous elevations of diverse temporal kinetics in brain water diffusion rate. Our current data are derived from 5 min apart acquisitions, providing information over the early phase of AQP4 inhibition therefore extending our early report (56). The regional heterogeneity likely reflects the various levels of AQP4 expression; its relative enrichment in the cerebral cortex (57) corresponds to the pronounced effect observed here by DW-MRI. An overall increase in brain water diffusion rate was observed when blocking AQP4 water efflux. This

treatment causes water accumulation inside astrocytes and their swelling, which reduces the extracellular space but increases the intracellular space. Water diffusion would be enhanced inside astrocytes and decreased in extracellular space, respectively. DW-MRI maps global water diffusion of both intra- and extracellular space. Likely, a net increase in brain water diffusion may reflect its intracellular increase exceeding the extracellular decrease. In addition, convective brain fluid flow has been suggested to be present in the perivascular space (52), a scenario extended by the glymphatic system to the extracellular space of the parenchyma (58). In this sense, squeezing of extracellular space might increase the rate of the water flow. The current MRI data yet lack sufficient spatial resolution to delineate the spatial compartmentalization of the brain fluid flow.

Our study sheds light on the mechanisms by which astrocyte aquaporin contributes to the water environment of brain parenchyma, and will help to understand the processes underlying the brain homeostasis and adaptation to life conditions.

Materials and methods

Experiments were undertaken in accordance with European Community guiding principles on the care and use of animals (86/609/CEE), and the rules of the host institute. For water transport and volume imaging, coronal slices comprising somatosensory cortex were acutely prepared from C57BL/6 mice of both sexes at ages of about 4-6 weeks, unless otherwise indicated. Light sheet and epifluorescence imaging were both performed on a wide-field upright microscope (Zeiss Axioskop 50, Germany). *In vivo* fiber photometry recording was performed using a Neurophotometrics system (FP3002). DW-MRI experiments were conducted on a Bruker 7T

scanner using a cryo-cooled mouse brain coil, mice being mildly anesthetized with medetomidine (0.6 mg/kg/h, intravenous injection). Extended methods are provided in *SI Appendix*.

Acknowledgements and funding sources

We thank the animal and imaging facilities of the IBPS (Sorbonne Université, Paris, France). We thank Nathalie Rouach for the GFAP-EGFP mice, Hervé Le Corronc and Thomas Panier for the discussion and the 3D printing of the light sheet chamber, respectively. This work was supported by the Agence Nationale de la Recherche (ANR-17-CE37-0010-03; ANR-20-CE14-0025-02), France Alzheimer individual fellowship (2021-2022), Japanese society for promotion of science (JSPS) 2022 summer grant, Grant-in-Aid for Challenging Research (Exploratory) in Japan (grant number 21K19464), the i-Bio initiative grant of Sorbonne Université.

Supporting Information

Extended methods and four supplementary figures (*SI Appendix,* Fig. S1-S4) are included.

Competing interest

The authors declare no competing financial interests.

Data sharing plans

The authors commit to share data, documentation, and code used in analysis.

References:

1. Kimelberg HK (2004) Water homeostasis in the brain: basic concepts. *Neuroscience* 129(4):851-860.
2. Brinker T, Stopa E, Morrison J, & Klinge P (2014) A new look at cerebrospinal fluid circulation. *Fluids Barriers CNS* 11:10.
3. Agnati LF, Marcoli M, Leo G, Maura G, & Guidolin D (2017) Homeostasis and the concept of 'interstitial fluids hierarchy': Relevance of cerebrospinal fluid sodium concentrations and brain temperature control (Review). *Int J Mol Med* 39(3):487-497.
4. Louveau A, *et al.* (2017) Understanding the functions and relationships of the glymphatic system and meningeal lymphatics. *J Clin Invest* 127(9):3210-3219.
5. Abbott NJ, Pizzo ME, Preston JE, Janigro D, & Thorne RG (2018) The role of brain barriers in fluid movement in the CNS: is there a 'glymphatic' system? *Acta Neuropathol* 135(3):387-407.
6. Le Bihan D, Urayama S, Aso T, Hanakawa T, & Fukuyama H (2006) Direct and fast detection of neuronal activation in the human brain with diffusion MRI. *Proceedings of the National Academy of Sciences of the United States of America* 103(21):8263-8268.
7. Gaddamanugu S, *et al.* (2022) Clinical applications of diffusion-weighted sequence in brain imaging: beyond stroke. *Neuroradiology* 64(1):15-30.
8. Le Bihan D & Iima M (2015) Diffusion Magnetic Resonance Imaging: What Water Tells Us about Biological Tissues. *PLoS Biol* 13(7):e1002203.
9. Papadopoulos MC & Verkman AS (2013) Aquaporin water channels in the nervous system. *Nat Rev Neurosci* 14(4):265-277.
10. Xiao M, Hou J, Xu M, Li S, & Yang B (2023) Aquaporins in Nervous System. *Adv Exp Med Biol* 1398:99-124.
11. Barres BA (2008) The mystery and magic of glia: a perspective on their roles in health and disease. *Neuron* 60(3):430-440.
12. Appaix F, *et al.* (2012) Specific in vivo staining of astrocytes in the whole brain after intravenous injection of sulforhodamine dyes. *PLoS One* 7(4):e35169.
13. Pham C, *et al.* (2020) Mapping astrocyte activity domains by light sheet imaging and spatio-temporal correlation screening. *Neuroimage* 220:117069.
14. Huber VJ, Tsujita M, & Nakada T (2009) Identification of aquaporin 4 inhibitors using in vitro and in silico methods. *Bioorg Med Chem* 17(1):411-417.
15. Burnett ME, Johnston HM, & Green KN (2015) Structural characterization of the aquaporin inhibitor 2-nicotinamido-1,3,4-thiadiazole. *Acta Crystallogr C Struct Chem* 71(Pt 12):1074-1079.
16. Toft-Bertelsen TL, *et al.* (2021) Clearance of activity-evoked K(+) transients and associated glia cell swelling occur independently of AQP4: A study with an isoform-selective AQP4 inhibitor. *Glia* 69(1):28-41.

17. Harrison IF, *et al.* (2020) Impaired glymphatic function and clearance of tau in an Alzheimer's disease model. *Brain* 143(8):2576-2593.

18. Igarashi H, Tsujita M, Suzuki Y, Kwee IL, & Nakada T (2013) Inhibition of aquaporin-4 significantly increases regional cerebral blood flow. *Neuroreport* 24(6):324-328.

19. Haj-Yasein NN, *et al.* (2011) Glial-conditional deletion of aquaporin-4 (Aqp4) reduces blood-brain water uptake and confers barrier function on perivascular astrocyte endfeet. *Proceedings of the National Academy of Sciences of the United States of America* 108(43):17815-17820.

20. Binder DK, Papadopoulos MC, Haggie PM, & Verkman AS (2004) In vivo measurement of brain extracellular space diffusion by cortical surface photobleaching. *J Neurosci* 24(37):8049-8056.

21. MacAulay N (2021) Molecular mechanisms of brain water transport. *Nat Rev Neurosci* 22(6):326-344.

22. Yao X, *et al.* (2015) Aquaporin-4 regulates the velocity and frequency of cortical spreading depression in mice. *Glia* 63(10):1860-1869.

23. Gomolka RS, *et al.* (2023) Loss of aquaporin-4 results in glymphatic system dysfunction via brain-wide interstitial fluid stagnation. *eLife* 12.

24. Benfenati V, *et al.* (2011) An aquaporin-4/transient receptor potential vanilloid 4 (AQP4/TRPV4) complex is essential for cell-volume control in astrocytes. *Proceedings of the National Academy of Sciences of the United States of America* 108(6):2563-2568.

25. Eilert-Olsen M, *et al.* (2019) Astroglial endfeet exhibit distinct Ca(2+) signals during hypoosmotic conditions. *Glia* 67(12):2399-2409.

26. Herrera Moro Chao D, *et al.* (2022) Hypothalamic astrocytes control systemic glucose metabolism and energy balance. *Cell metabolism* 34(10):1532-1547 e1536.

27. Fiacco TA, *et al.* (2007) Selective stimulation of astrocyte calcium in situ does not affect neuronal excitatory synaptic activity. *Neuron* 54(4):611-626.

28. Yang J, *et al.* (2019) Glutamate-Releasing SWELL1 Channel in Astrocytes Modulates Synaptic Transmission and Promotes Brain Damage in Stroke. *Neuron*.

29. Karagiannis A, *et al.* (2021) Lactate is an energy substrate for rodent cortical neurons and enhances their firing activity. *eLife* 10.

30. Cauli B, *et al.* (2000) Classification of fusiform neocortical interneurons based on unsupervised clustering. *Proceedings of the National Academy of Sciences of the United States of America* 97(11):6144-6149.

31. Taniguchi H, *et al.* (2011) A resource of Cre driver lines for genetic targeting of GABAergic neurons in cerebral cortex. *Neuron* 71(6):995-1013.

32. Ochoa-de la Paz LD & Gulias-Canizo R (2022) Glia as a key factor in cell volume regulation processes of the central nervous system. *Front Cell Neurosci* 16:967496.

33. Zhao HH, *et al.* (2019) Time-resolved quantification of the dynamic extracellular space in the brain: study of cortical spreading depression. *Journal of neurophysiology* 121(5):1735-1747.

34. Holthoff K & Witte OW (1996) Intrinsic optical signals in rat neocortical slices measured with near-infrared dark-field microscopy reveal changes in extracellular space. *J Neurosci* 16(8):2740-2749.

35. Gorski JA, *et al.* (2002) Cortical excitatory neurons and glia, but not GABAergic neurons, are produced in the Emx1-expressing lineage. *J Neurosci* 22(15):6309-6314.

36. Madisen L, *et al.* (2012) A toolbox of Cre-dependent optogenetic transgenic mice for light-induced activation and silencing. *Nat Neurosci* 15(5):793-802.

37. Chung DY, *et al.* (2019) Determinants of Optogenetic Cortical Spreading Depolarizations. *Cereb Cortex* 29(3):1150-1161.

38. MacVicar BA & Hochman D (1991) Imaging of synaptically evoked intrinsic optical signals in hippocampal slices. *J Neurosci* 11(5):1458-1469.

39. Beaulieu C (2002) The basis of anisotropic water diffusion in the nervous system - a technical review. *NMR Biomed* 15(7-8):435-455.

40. Le Bihan D (2014) Diffusion MRI: what water tells us about the brain. *EMBO Mol Med* 6(5):569-573.

41. Dallerac G, Zapata J, & Rouach N (2018) Versatile control of synaptic circuits by astrocytes: where, when and how? *Nat Rev Neurosci* 19(12):729-743.

42. Cauli B, Dusart I, & Li D (2023) Lactate as a determinant of neuronal excitability, neuroenergetics and beyond. *Neurobiol Dis*:106207.

43. Bonvento G & Bolanos JP (2021) Astrocyte-neuron metabolic cooperation shapes brain activity. *Cell metabolism* 33(8):1546-1564.

44. Noda Y, Sohara E, Ohta E, & Sasaki S (2010) Aquaporins in kidney pathophysiology. *Nat Rev Nephrol* 6(3):168-178.

45. Jeon H, *et al.* (2021) Upregulation of AQP4 Improves Blood-Brain Barrier Integrity and Perihematomal Edema Following Intracerebral Hemorrhage. *Neurotherapeutics* 18(4):2692-2706.

46. Mireles-Ramirez MA, *et al.* (2022) Neuromyelitis optica spectrum disorder: pathophysiological approach. *Int J Neurosci*:1-13.

47. Lucchinetti CF, *et al.* (2014) The pathology of an autoimmune astrocytopathy: lessons learned from neuromyelitis optica. *Brain Pathol* 24(1):83-97.

48. Amiry-Moghaddam M, *et al.* (2003) An alpha-syntrophin-dependent pool of AQP4 in astroglial end-feet confers bidirectional water flow between blood and brain. *Proceedings of the National Academy of Sciences of the United States of America* 100(4):2106-2111.

49. Murphy TR, *et al.* (2017) Hippocampal and Cortical Pyramidal Neurons Swell in Parallel with Astrocytes during Acute Hypoosmolar Stress. *Front Cell Neurosci* 11:275.

50. Mola MG, *et al.* (2016) The speed of swelling kinetics modulates cell volume regulation and calcium signaling in astrocytes: A different point of view on the role of aquaporins. *Glia* 64(1):139-154.

51. Woo J, *et al.* (2018) Astrocytic water channel aquaporin-4 modulates brain plasticity in both mice and humans: a potential gliogenetic mechanism underlying language-associated learning. *Mol Psychiatry* 23(4):1021-1030.

52. Smith AJ & Verkman AS (2019) CrossTalk opposing view: Going against the flow: interstitial solute transport in brain is diffusive and aquaporin-4 independent. *J Physiol* 597(17):4421-4424.

53. Smith AJ, Yao X, Dix JA, Jin BJ, & Verkman AS (2017) Test of the 'glymphatic' hypothesis demonstrates diffusive and aquaporin-4-independent solute transport in rodent brain parenchyma. *eLife* 6.

54. Mestre H, *et al.* (2018) Aquaporin-4-dependent glymphatic solute transport in the rodent brain. *eLife* 7.

55. Rasmussen MK, Mestre H, & Nedergaard M (2022) Fluid transport in the brain. *Physiol Rev* 102(2):1025-1151.

56. Debacker C, Djemai B, Ciobanu L, Tsurugizawa T, & Le Bihan D (2020) Diffusion MRI reveals in vivo and non-invasively changes in astrocyte function induced by an aquaporin-4 inhibitor. *PLoS One* 15(5):e0229702.

57. Clarke LE, *et al.* (2018) Normal aging induces A1-like astrocyte reactivity. *Proceedings of the National Academy of Sciences of the United States of America* 115(8):E1896-E1905.

58. Mestre H, *et al.* (2018) Flow of cerebrospinal fluid is driven by arterial pulsations and is reduced in hypertension. *Nature communications* 9(1):4878.

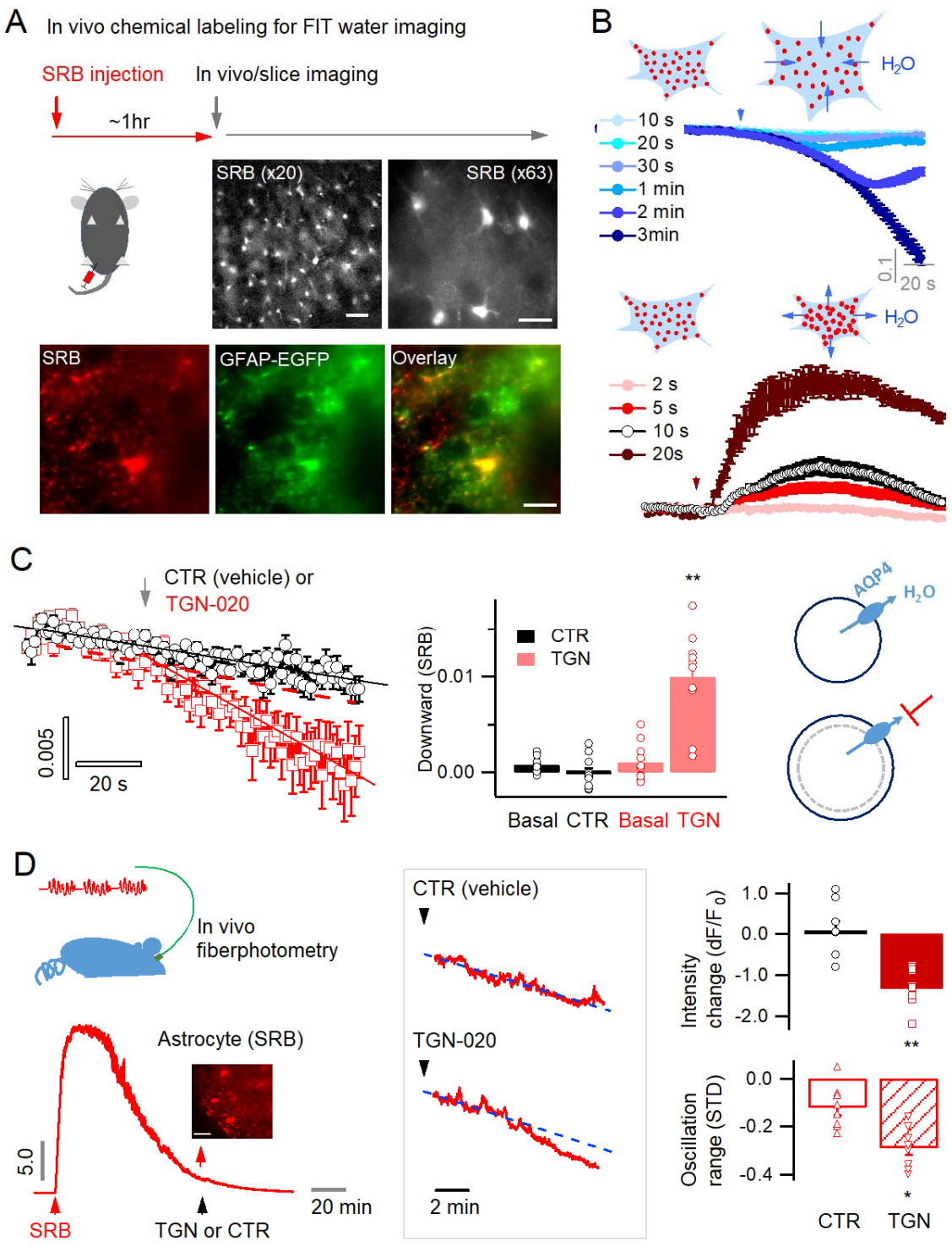

FIGURE 1

Fig. 1. Astrocyte aquaporin mediates a tonic water efflux. (*A*) *In vivo* chemical labelling of astrocytes. Sulforhodamine B (SRB, 10 mg/ml) was intraperitoneally injected in awake mice (10 µl/g). Monochrome images show representative astrocyte labeling in living acute brain slices from cortex under low (×20; scale bar, 50 µm) and high magnification (×63; scale bar, 20 µm) by epifluorescence. *Below*, SRB labeling was confirmed to be astrocyte-specific in acute brain slices of the astrocyte reporter line GFAP-EGFP, where light sheet imaging was used to gain optical sectioning (*SI Appendix*, Extended methods and Fig. S1). Scale bar, 20 µm. (*B*) Optical imaging of astrocyte water transport *in situ* in acute brain slices. Transmembrane water transport was triggered with hypo- and hypertonic solution, inducing water inflow and outflow that were respectively reflected by SRB fluorescence decrease and increase. Different durations of application of the hypo- or hypertonic solution caused water transport of different extents, translated by SRB fluorescence time courses of distinct amplitudes (n = 52 astrocytes, 4 mice). (*C*) Acutely blocking astrocyte AQP4 with TGN-020 caused intracellular water accumulation and swelling. *Left*, while no effect was seen under CTR condition (vehicle only, n = 23 astrocytes), TGN-020 (20 µM) significantly decreased astrocyte SRB fluorescence (n = 30, 6 mice). Imaging was performed in acute brain slices of layer II/III S1 cortex. *Middle*, the downward slope was compared between the periods before and after the application of TGN-020. *Right*, illustration shows astrocyte aquaporin sustaining a tonic water efflux. Its blockade causes water accumulation and cell swelling. (*D*) *In vivo* validation of the effect of TGN-020 application on astrocyte water homeostasis. *Left*, fiber photometry was used for real-time recording of SRB fluorescence of astrocyte population in S1 cortex in freely moving mice, with saline (CTR) or TGN-020 being intraperitoneally injected when SRB was trapped in astrocytes. Fiber photometry recording shows that *in vivo* SRB injection resulted in rapid entry into mouse cortex and, in about one hour, led to astrocyte labeling (inset scale bar, 50 µm). *Middle*, example response to saline and TGN-020. Relative to CTR, TGN caused a decrease in astrocyte SRB fluorescence and its oscillation range (n = 8 recordings per condition, 5 mice).

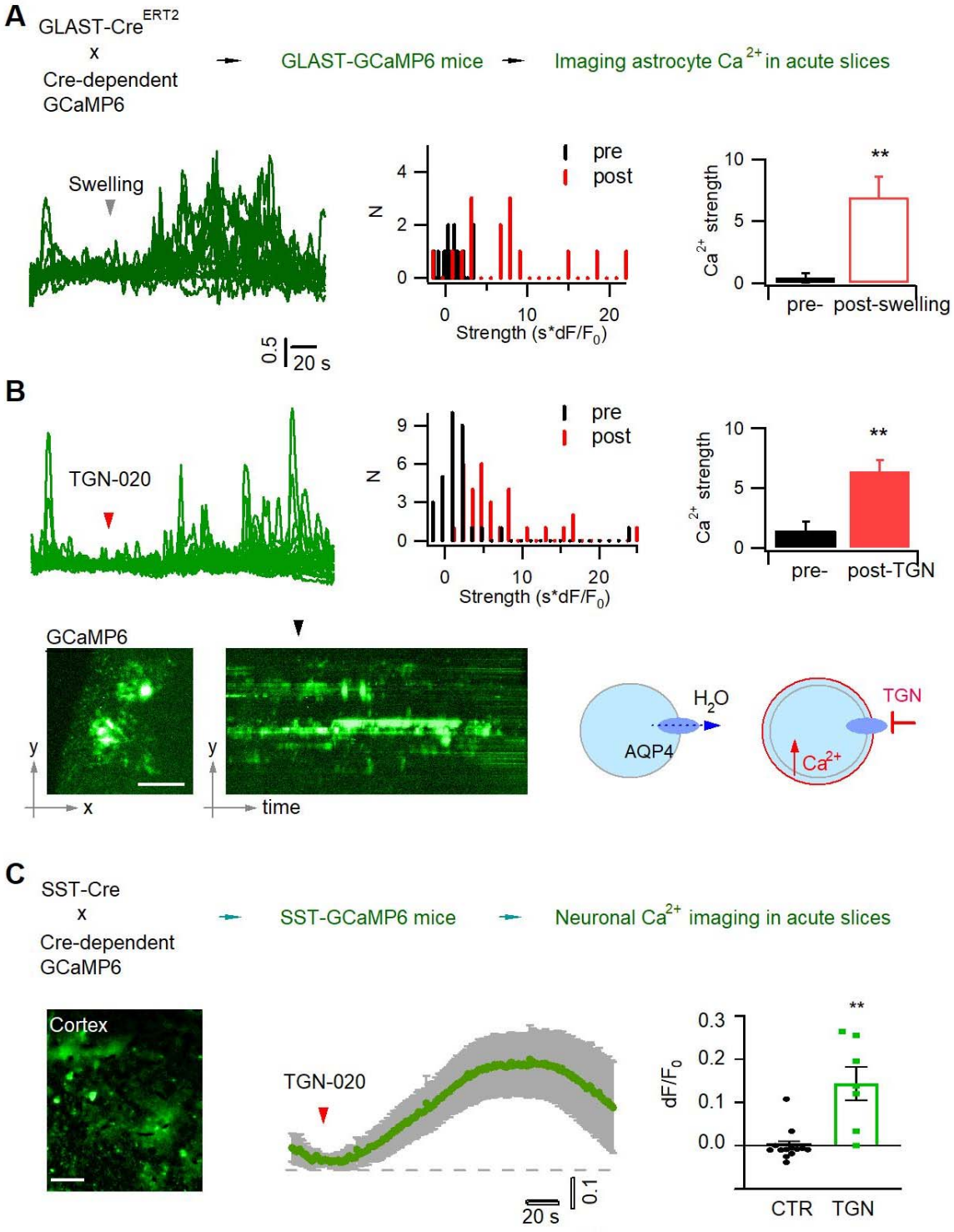

FIGURE 2

Fig. 2. Acutely blocking astrocyte aquaporin induces swelling-associated Ca^{2+} oscillation. (*A*) *In vivo* expression in astrocytes of the genetically encoded fluorescent Ca^{2+} indicator GCaMP6 for imaging astrocyte Ca^{2+} in acute brain slices. Light sheet microscopy was used to capture transient Ca^{2+} signals of local regions. As a positive control, astrocyte swelling was induced by hypotonic solution (100 mOsM) that caused Ca^{2+} changes from their homeostatic level. *Left*, representative time courses of swelling-induced Ca^{2+} changes in detected response regions; *middle to left*, the histogram distribution and bar representation showing the signal strengths that were derived from the temporal integral of individual Ca^{2+} time courses normalized per minute, before and after cell swelling (n = 15 astrocytes of three mice). (*B*) Astrocyte Ca^{2+} oscillation caused by acute aquaporin blocking with TGN-020 (n = 31 astrocytes of 5 mice), due to the inhibition of the tonic water efflux that led to astrocyte swelling as illustrated. Scale bar, 50 μm. (*C*) Intercellular effect on SST interneurons of blocking astrocyte aquaporin water efflux. TGN-020 (20 μM) or the equal molar vehicle (CTR) was bath applied to acute cortical slices of SST-GCaMP6 mice (n = 7-12 measurements from 4 mice). Scale bar, 50 μm.

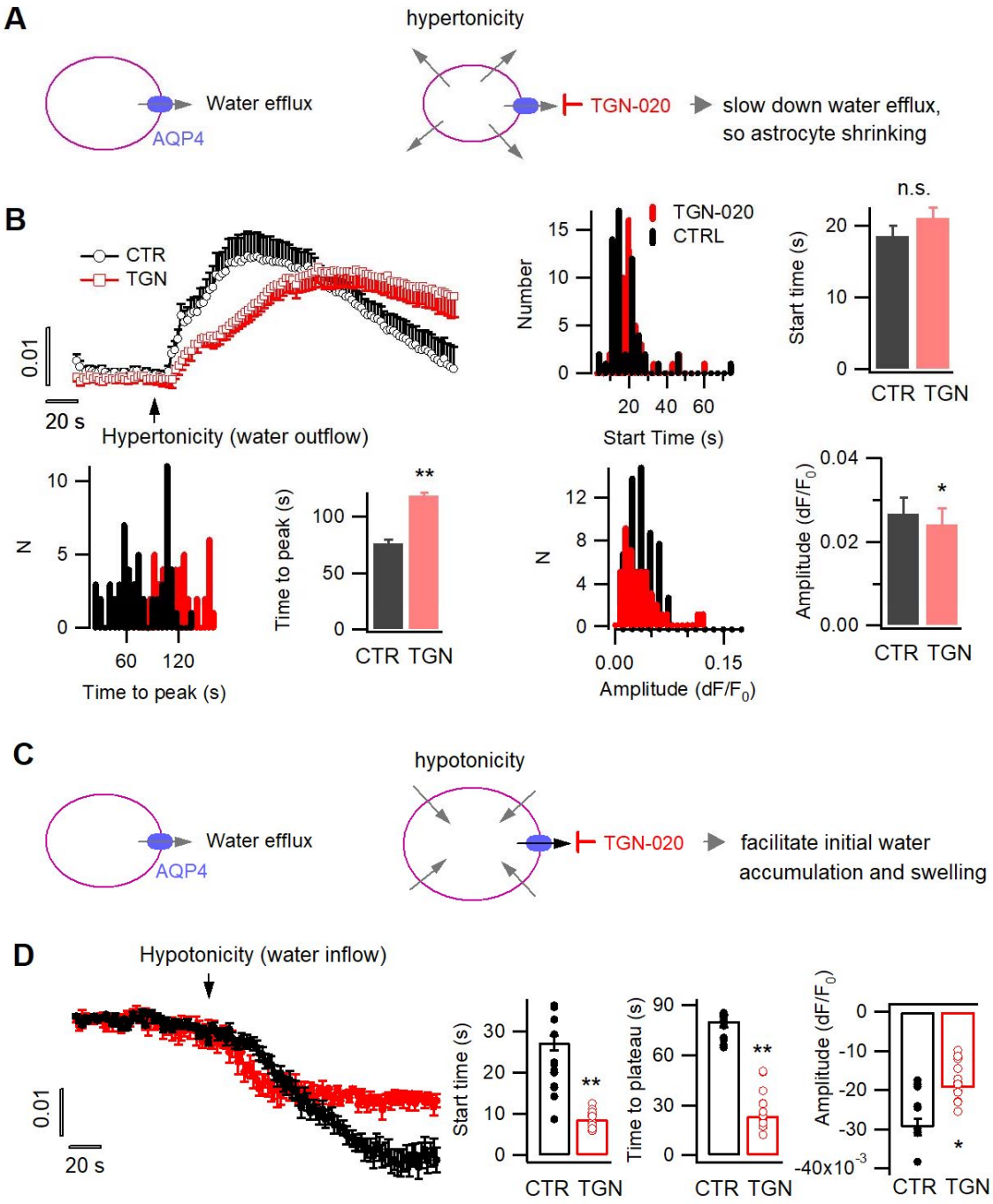

FIGURE 3

Fig. 3. Tonic water efflux via aquaporin modulates phasic transmembrane water transport and astrocyte volume response. (*A*) *Left*, in basal condition astrocyte aquaporin mediates a tonic water efflux. *Right*, protocol to induce water outflow from astrocytes, therefore their shrinking, by hypertonic extracellular solution (400 mOsM) in either control condition (CTR) or in the presence of AQP4 inhibitor TGN-020 (20 µM). (*B*) Time courses of astrocyte SRB fluorescence increase upon the phasically induced water outflow, reflecting the occurrence of shrinking. The histograms and bar charts compare the start time, namely the delay between hypertonic solution application and rise in SRB fluorescence, the time to reach the peak of shrinking, and the absolute amplitude of water outflow-induced SRB increase (n = 58 astrocytes for CTR, and 47 astrocytes for TGN-020, four mice). (*C*) *Right*, protocol to trigger water inflow into astrocytes by hypotonic extracellular solution (100 mOsM) in either CTR solution or in the presence of TGN-020 (20 µM). (*D*) Time courses of astrocyte SRB fluorescence decrease caused by water inflow, which also reflects concomitant cell swelling. In contrast to the observation with hypertonicity-induced water outflow and astrocyte shrinking, a reduction was observed for both the start time and the time-to-peak with TGN-020 (n = 12 astrocytes for CTR, and 12 astrocytes for TGN-020, four mice). TGN-020 led to a decrease in the absolute amplitude of astrocyte swelling.

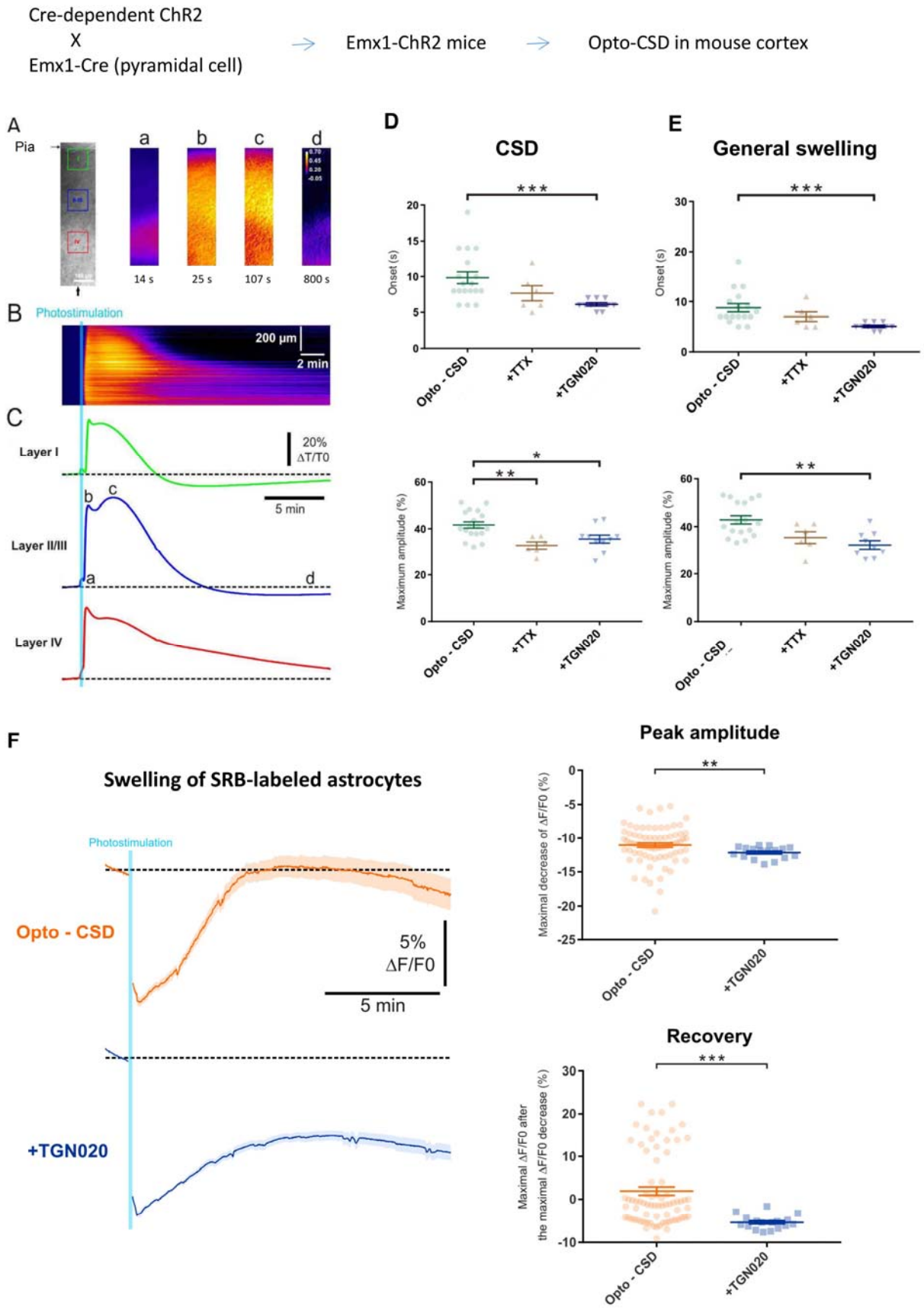

FIGURE 4

Fig. 4. AQP4-mediated tonic water outflow regulates global swelling in cortical parenchyma. CSD-associated general swelling was induced by photostimulating ChR2-expressing pyramidal cells in acute cortical slices, and recorded by imaging intrinsic optical signal (IOS) with infrared illumination. (*A*) Representative recording. The pia surface is on the upper side; green, blue and red squares correspond to regions of interest in Layers I, II-III and IV, respectively. Transmittance signals are represented in pseudocolor images at different time points post photostimulation. Scale bar, 100 µm. (*B*) Kymograph showing the IOS changes in a radial line of interest indicated by a black arrow in *A*. The light blue line indicates the 10-s photostimulation that increases the infrared transmittance signal (dT/T_0) across cortical layers, as also illustrated by the time courses; *a*, *b*, *c* and *d* correspond to the time points depicted in *A*. After the onset delay (*a*), the first (*b*) and second (*c*) peak of IOS are characteristic of the CSD and a prolonged general swelling, respectively. (*D-E*) TGN-020 (20 µM) inhibition of AQP4 reduced the initial onset and the maximal amplitude of both the CSD and general swelling (n = 6 - 18 measurements from 13 mice per condition) in layer II/III cortex. Inhibiting spiking activity with TTX (1 µM) only affected the amplitude of the initial CSD response. (*F*) Astrocytes swelling, reflected by SRB fluorescence decrease, monitored in control condition (n = 75 astrocytes) and in the presence of TGN-020 (n = 17 astrocytes) in layer II/III cortex.

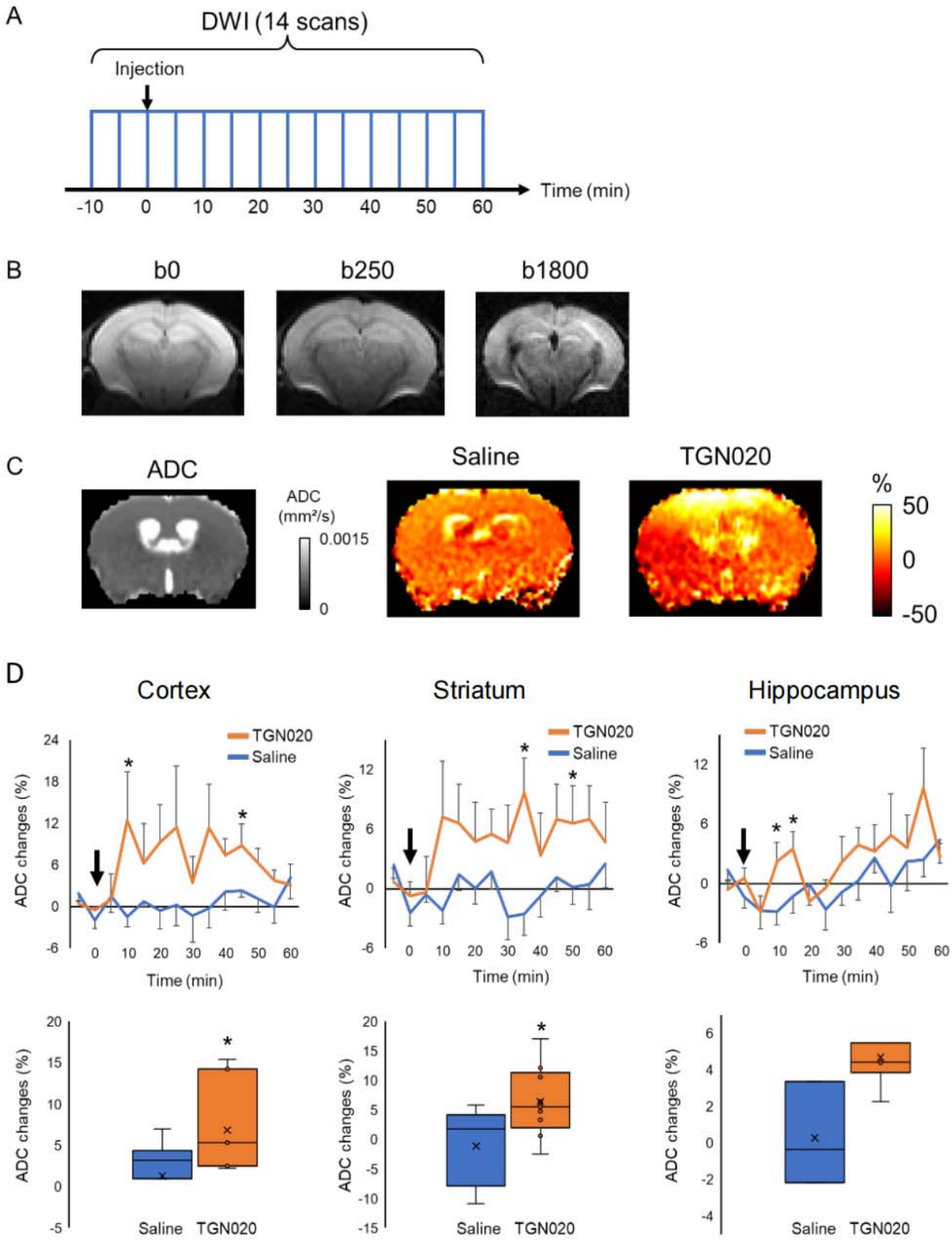

FIGURE 5

Fig. 5. Perturbing the tonic water efflux via astrocyte aquaporin alters brain water homeostasis. *In vivo* DW-MRI (7T) was employed to map water diffusion in the entire brain scale following the acute inhibition of astrocytic AQP4 (TGN-020, intraperitoneal injection, 200 mg/kg), with paralleled control experiments performed with saline injection. (*A*) Experimental protocol for DW-MRI. Saline or TGN020 was injected at 10 min after the start of acquisition. DWI was acquired every 5 min. (*B*) Representative image obtained at three different b values to derive the water diffusion rates. (*C*) *Left*, brain water diffusion rate was mapped by the calculation of apparent diffusion coefficient (ADC). *Right*, representative images illustrating the relative changes of ADC at 60 min after injection of saline or TGN-020. (*D*) Time courses depicting the temporal changes in ADC in the cortex, striatum, and hippocampus, revealing the regional heterogeneity. Arrowhead indicates the injection of saline or TGN-020 (n = 10 mice for saline injection, 9 mice for TGN-020).